POLITECNICO DI TORINO
Repository ISTITUZIONALE

Plasma edge and plasma-wall interaction modelling: Lessons learned from metallic devices

Original
Plasma edge and plasma-wall interaction modelling: Lessons learned from metallic devices / Wiesen, S., Groth, M., Wischmeier, M., Brezinsek, S., Jarvinen, A., Reimold, F., Aho-Mantila, L., Subba, F., Jet, C.. - In: NUCLEAR MATERIALS AND ENERGY. - ISSN 2352-1791. - 12:(2017), pp. 3-17. [10.1016/j.nme.2017.03.033]

Availability:
This version is available at: 11583/3017383 since: 2026-11-02T09:39:02Z

Publisher:
Elsevier Ltd

Published
DOI:10.1016/j.nme.2017.03.033

Terms of use:

This article is made available under terms and conditions as specified in the corresponding bibliographic description in the repository

Publisher copyright

(Article begins on next page)

28 November 2026

Aalto University

OPEN ACCESS

This is an electronic reprint of the original article.
This reprint may differ from the original in pagination and typographic detail.

Wiesen, S.; Groth, Mathias; Wischmeier, M.; Brezinsek, S.; Jarvinen, A.; Reimold, F.; Aho-Mantila, L.; JET Contributors; The EUROfusion MST1 team; The ASDEX Upgrade team; The Alcator C-mod team

Plasma edge and plasma-wall interaction modelling

Published in:
Nuclear Materials and Energy

DOI:
10.1016/j.nme.2017.03.033

E-pub ahead of print: 01/01/2017

Document Version
Version created as part of publication process; publisher's layout; not normally made publicly available

Please cite the original version:
JET Contributors, The EUROfusion MST1 team, The ASDEX Upgrade team, & The Alcator C-mod team (2017). Plasma edge and plasma-wall interaction modelling: Lessons learned from metallic devices. Nuclear Materials and Energy. DOI: 10.1016/j.nme.2017.03.033

This material is protected by copyright and other intellectual property rights, and duplication or sale of all or part of any of the repository collections is not permitted, except that material may be duplicated by you for your research use or educational purposes in electronic or print form. You must obtain permission for any other use. Electronic or print copies may not be offered, whether for sale or otherwise to anyone who is not an authorised user.

Nuclear Materials and Energy 000 (2017) 1–15

Contents lists available at ScienceDirect

Nuclear Materials and Energy

journal homepage: www.elsevier.com/locate/nme

Plasma edge and plasma-wall interaction modelling: Lessons learned from metallic devices

S. Wiesen[a,*], M. Groth[b], M. Wischmeier[c], S. Brezinsek[a], A. Jarvinen[d], F. Reimold[a], L. Aho-Mantila[e], JET contributors[f,1], The EUROfusion MST1 team[2], The ASDEX Upgrade team[c], The Alcator C-mod team[g]

[a] Forschungszentrum Jülich GmbH, Institut für Energie- und Klimaforschung – Plasmaphysik, 52425 Jülich, Germany
[b] Aalto University, Espoo, Finland
[c] Max-Planck-Institut für Plasmaphysik, 85748 Garching bei München, Germany
[d] Lawrence Livermore National Laboratory, Livermore, CA 94550, USA
[e] VTT Technical Research Centre of Finland Ltd, P.O. Box 1000, FI-02044 VTT, Finland
[f] EUROfusion Consortium, JET, Culham Science Centre, Abingdon, OX14 3DB, UK
[g] Plasma Science and Fusion Centre, MIT, Cambridge, MA 02139, USA

ARTICLE INFO

Article history:
Received 3 July 2016
Revised 10 February 2017
Accepted 21 March 2017
Available online xxx

ABSTRACT

Robust power exhaust schemes employing impurity seeding are needed for target operational scenarios in present day tokamak devices with metallic plasma-facing components (PFCs). For an electricity-producing fusion power plant at power density $P_{sep}/R > 15$ MW/m divertor detachment is a requirement for heat load mitigation. 2D plasma edge transport codes like the SOLPS code as well as plasma-wall interaction (PWI) codes are key to disentangle relevant physical processes in power and particle exhaust. With increased quantitative credibility in such codes more realistic and physically sound estimates of the life-time expectations and performance of metallic PFCs can be accomplished for divertor conditions relevant for ITER and DEMO. An overview is given on the recent progress of plasma edge and PWI modelling activities for (carbon-free) metallic devices, that include results from JET with the ITER-like wall, ASDEX Upgrade and Alcator C-mod. It is observed that metallic devices offer an opportunity to progress the understanding of underlying plasma physics processes in the edge. The validation of models can be substantially improved by eliminating carbon from the experiment as well as from the numerical system with reduced degrees of freedom as no chemical sputtering from amorphous carbon layers and no carbon or hydro-carbon transport are present. With the absence of carbon as the primary plasma impurity and given the fact that the physics of the PWI at metallic walls is less complex it is possible to isolate the crucial plasma physics processes relevant for particle and power exhaust. For a reliable 2D dissipative plasma exhaust model these are: cross-field drifts, complete kinetic neutral physics, geometry effects (including main-chamber, divertor and sub-divertor structures), SOL transport reflecting also the non-diffusive nature of anomalous transport, as well as transport within the pedestal region in case of significant edge impurity radiation affecting pedestal pressure and hence P_{sep}.

© 2017 Published by Elsevier Ltd.
This is an open access article under the CC BY-NC-ND license.
(http://creativecommons.org/licenses/by-nc-nd/4.0/)

1. Introduction

Tokamak devices with metallic plasma-facing components (PFCs) have demonstrated to perform successfully preserving the first wall [1]. It has been shown that long-term fuel retention can be minimised [2] and metallic PFCs do allow for fast isotope exchange [3]. However, armour materials like tungsten or W-coated CFC have significantly lower heat load limits restricted by melting, embrittlement and recrystallization effects compared to graphite/CFC PFCs. Also, W-sputtering and an unfavourable neoclassical transport of W-impurities can possibly lead to W accumulation which requires adequate avoidance techniques, at least for existing devices (it should be noted that neoclassical W transport in the ITER pedestal is now suspected to be not too unfavourable due to a different ratio of pedestal n- and T-gradients, c.f. [4]). Due

* Corresponding author.
E-mail address: s.wiesen@fz-juelich.de (S. Wiesen).

[1] See the Appendix of F. Romanelli et al., Proceedings of the 25th IAEA Fusion Energy Conference 2014, Saint Petersburg, Russia

[2] See http://www.euro-fusionscipub.org/mst1

http://dx.doi.org/10.1016/j.nme.2017.03.033
2352-1791/© 2017 Published by Elsevier Ltd. This is an open access article under the CC BY-NC-ND license. (http://creativecommons.org/licenses/by-nc-nd/4.0/)

Please cite this article as: S. Wiesen et al., Plasma edge and plasma-wall interaction modelling: Lessons learned from metallic devices, Nuclear Materials and Energy (2017), http://dx.doi.org/10.1016/j.nme.2017.03.033

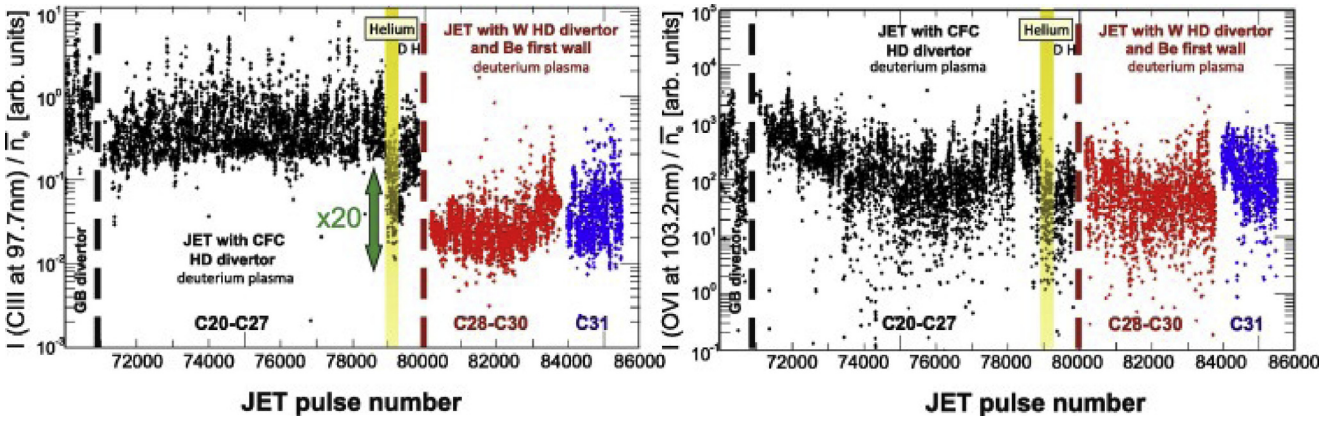

Fig. 1. From JET-C to JET ILW: C (CIII/neCIII/ne) and O edge plasma content (OVI/neOVI/ne) during the divertor phase as function of discharge number (reproduced from [8]).

to the lack of the intrinsic carbon radiator in present day metallic devices, discharges at high power require reliable exhaust schemes employing low-Z (Ne, N) or medium-Z (Ar, Kr, Xe) impurity seeding. For an electricity-producing fusion power plant at power density $P_{sep}/R > 15$ MW/m divertor detachment ($T_{e,plate} << 5$ eV and low saturation current j_{sat}) is an additional requirement for heat load mitigation [5]. To meet such constraints in ITER or DEMO, a significant fraction of the power P_{SOL} arriving in the SOL must be dissipated, and a radiative dissipation fraction $f_{rad} = P_{rad}/P_{SOL}$ of about 60% in ITER and exceeding 95% in DEMO (with 70% core radiation) is aimed for.

As no simple scaling for the particle and power exhaust problem exists, computational tools like the SOLPS edge plasma code [6] (or similar 2D or 3D edge codes) and plasma-wall interaction (PWI) codes are key for realistic and physically sound estimates of the life-time expectations and performance of metallic PFCs relevant for ITER and DEMO. This can only be accomplished when the numerically implemented physical model is sound, complete and the relevant physics processes have been identified, disentangled and understood. Challenging the employed numerical models against existing experiments is central for the validation process and important to increase quantitative credibility in the codes.

The carbon content in a metallic device like JET has been massively reduced either by using He-discharges in JET-C (factor 7) or the use of D in the ILW (factor 10–20) which was related to an effective disabling of the carbon erosion process [7,8] (c.f. Fig. 1). As a consequence of the reduction of the C-content it has been reported that in case of a carbon device like JET-C some of the relevant physics in the edge/SOL and plasma-wall interaction was masked by the impact of C on the plasma [8]. Thus, metallic devices offer an opportunity to progress the understanding of underlying plasma physics processes in the edge. Edge plasma and PWI modelling attempts suffered substantially from unknowns in the behaviour of the amorphous carbon PFC surfaces making a quantitative analysis of carbon transport and migration as well as the impact on the main plasma difficult. With the absence of carbon as the primary plasma impurity and radiator it is possible to eliminate some of the free parameters for impurity transport from the models (i.e. chemical sputtering and consequences from hydro-carbon transport physics and retention in amorphous carbon layers). Hence, with the metallic devices it seems to be simpler to disentangle the crucial processes relevant for particle and power exhaust from the impact of carbon transport physics otherwise observed in devices with C as PFCs [5].

High power tokamak operations with high-Z metallic PFCs are more susceptible to PWI as the influx of sputtered high-Z material into the confined region must be kept low to avoid accumulation [1]. Contrary to C, the process of W or Mo production by physical sputtering is well described by existing models [9,10] and thus may be regarded as understood. On top, high-Z impurities barely affect the edge plasma itself and transport can be treated by using existing kinetic models [11–13] or fluid models assuming some reduction in physics [14]. Low-Z material production on the other hand differs from high-Z as additional chemical processes might occur that might impact the total impurity influx (e.g. physical sputtering of Be and chemically assisted BeD production [7]).

Over the recent years it has become evident that the demand in understanding of PWI employing material transport as well as melt and dust codes has risen since the establishment of metallic PFCs in present day devices. Metallic surfaces do melt if they receive excessive heat loads and melt splashes can create droplet particles. As the mobility for those particles is low they are of no of large concern [15] but still reliable techniques for example for disruption mitigation are required to avoid major damage [16]. Otherwise, mobilisable dust created for example by arcings are an issue as it may cause explosion in the event of catastrophic loss of vacuum and subsequent air ingress in the vessel (loss of vacuum accidents, LOVAs [17]).

Compared to a C-wall, metallic surfaces have larger particle and energy reflection coefficients as calculated for example by TRIM calculations [9]. As it turns out, the impact of ballistically reflected neutrals on the ionisation source profile of the main plasma and the inclusion of kinetic neutral effects into edge transport codes is thus mandatory for an accurate description of plasma fuelling. Co-deposits can retain fuel effectively and subsequently release fuel into the main plasma by re-erosion of material. With the lack of carbon and with metallic PFCs such a ubiquitous fuel particle surface source or sink does not exist anymore. As a consequence, the poloidal fuelling profile becomes more localised in a metal device [18]. The overall impact of a metallic walls on pedestal fuelling and thus confinement is currently not well understood. Current hypotheses range from atomic physics effects and radiation at lower pedestal Z_{eff} [19], overall changes in pedestal transport and MHD and thus pedestal structure in presence of a metallic wall [20,21] as well as retarded fuelling effects by short time-scale outgassing dynamics during ELMs at the metallic PFCs [22,23]. A final conclusion about the fundamental reason for the change in confinement in metal devices is still pending.

In this review paper a summary is given on the consequences on the plasma edge modelling taking into account the change of PWI physics when going from C to metal PFCs. Without having the complexity to model carbon chemical and physical sputtering, neglecting the variation in stickiness for C atoms, hydrocarbons and molecular radicals, no long range migration and carbon co-

Please cite this article as: S. Wiesen et al., Plasma edge and plasma-wall interaction modelling: Lessons learned from metallic devices, Nuclear Materials and Energy (2017), http://dx.doi.org/10.1016/j.nme.2017.03.033

deposited layers and their erosion, metal devices seem to be simpler in terms of PWI physics compared to carbon devices. It will be shown that if one keeps other important aspects like for example neutral kinetics in the physics model for the edge or plasma drifts, the overall credibility and validity in the overall edge numerical model can be improved.

The structure of this review is organized as follows: Section 2 recapitulates used models for particle- and power physics and plasma detachment in nearly carbon free environments, i.e. JET, AUG and C-Mod (note that for example in AUG carbon is still present at a low level). Section 3 discusses briefly the recovery of power fall-off lengths using edge codes, i.e. the basic features required for reliable edge numerical models, highlighting that these do not differ much when going from C to metal PFCs. In Section 4 the necessary ingredients of a robust edge model describing the full cycle of the transition into divertor detachment in L- and H-mode are discussed and summarized. Section 5 discusses the criticality of neutral transport and highlights the issue to match the divertor neutral pressure as an important milestone in the validation process. Section 6 discusses the need for more global models integrating core/edge/PWI physics. The required revision of PWI models when moving from a carbon device to a metal device is highlighted and discusses the integration of relevant physics processes for material migration and transport being part of the overall edge plasma model. Section 7 concludes the paper with the lessons learned and gives recommendations about how to use edge codes to model particle and power exhaust in metallic devices.

2. Modelling power exhaust and divertor detachment in a carbon free environment

In a synthetic description of the power exhaust problem the energy dissipation in the plasma edge can be described as a step-ladder process [24]. Power from the confined region enters the plasma edge by anomalous cross-field transport (turbulent ballooning-like and/or laminar drift-driven) and is mainly conducted along temperature gradients within the scrape-off-layer (SOL). As the plasma accelerates towards the target plates a fraction of the heat flux is driven by convection and thus may be impacted by plasma drift flows. As energy is transported along the magnetic field lines downstream towards the divertor it reaches an impurity radiation zone at which the temperature T is reduced and thus the heat-flux. As T is decreasing and after passing the ionization front at $T_e \sim 5$ eV pressure is removed from the plasma by friction processes occurring between the plasma and the compressed divertor neutrals. Additionally, plasma particles are lost by transverse transport as well as charge-exchange (CX) processes, the latter leading to a spreading of energy by fast neutral particles. In the case that sufficient power could be radiated or dissipated away before reaching the target plate, T can be further reduced to $<<$ 2 eV by strong volume recombination processes which cause a further loss of plasma particles. A transition into the detached regime is characterized by a roll-over of the plate particle flux which will effectively reduce the target heat load even further as fewer particles recombine at the target plate surfaces (i.e. a smaller number of particles deposit their recombination energy of 13.6 eV + 2.3 eV when D^+ is converted to D_2 at the wall). Additional particle loss, like enhanced perpendicular transport or energy loss by other atomic processes, are acting as catalysers in the increase of the degree of detachment [25–27].

For the highly non-linear process of dissipation by divertor detachment no general scaling is available ([5] and references therein). Some detachment criteria exists which are, depending on the assumed interpretation of experimental data, can be seen as more or less heuristic [28–30]. For a proper model based treatment the application of at least two-dimensional edge codes is required, i.e. employing codes like SOLPS-ITER [31], EDGE2D-EIRENE [32–34], SOLEDGE2D-EIRENE [35], SONIC [36,37], UEDGE [38]. Other codes like OSM-EIRENE [39] exist for which experimental plasma profiles are taken as model constraint input to derive for example transport coefficients. All such computational fluid codes have in common that Bragisnkii-like equations are solved for electron and ion energy, parallel ion momentum and particle balances for all species on a 2D non-orthogonal rectangular grid. Usually, a discrimination is done between the parallel (to the field) and the radial (perpendicular to the field) motion of the plasma as the nature of transport is different along the two directions (classical parallel vs. anomalous radial). At all grid edges boundary conditions must be provided in order to find a unique numerical solution of the full fluid equation system. Common to all aforementioned edge codes is an iterative (sometimes time-dependent) coupling to the Monte-Carlo neutral kinetics codes like EIRENE [33], DEGAS [40] or NEUT2D [41] which solve the kinetic transport equations of Boltzmann-type providing the plasma source and loss terms within the volume and from the interaction at the numerical system boundaries, i.e. the walls. As neutral particles are not bound to the magnetic field a 3D toroidal approximation of the neutral simulation grid is usually applied. The mean-free path of the neutrals can be large at low T_e (i.e. the Knudsen number $Kn >> 1$ in detached conditions) and thus geometric details become relevant to identify the neutral pressure in the divertor. A kinetic approach for neutral transport is thus indispensable which allows (apart from the inclusion of relevant atomic and molecular physics processes details) the inclusion of geometric effects as well as accounting of non-equilibrium distribution functions.

In order to assess the predictive capability of a model for the power exhaust problem in ITER and DEMO, the codes must be first validated against real experimental data. Unknowns in the model setup however hamper the validation process. For example an anomalous transport parameter for the perpendicular direction must be prescribed in an ad-hoc way as consistent coupling schemes of edge codes with turbulence codes do not exist (or are still in development [42]). Transport in the parallel direction in case of strong gradients is not ideally described by a fluid approach and kinetic corrections (so called flux limiting factors) for heat and viscous flux have been implemented [6]. Other model parameters to describe the boundary condition towards walls normally have to be prescribed too (e.g. decay parameters for density and temperature). In some cases a model exists which describes the plasma up to the wall e.g. by grid extensions [35] and inclusion of a model for the sheath for glancing field line angles [43]. Sheath physics in general plays a significant role for the power balance. Usually fixed so called sheath heat transmission factors $\gamma_{e,i}$ are used to impose heat fluxes at the target surface $q^{targ}_{e,i} = \gamma_{e,i} \Gamma^{targ} T_{e,i}$ (with a combined $\gamma = \gamma_{i+}\gamma_e$ for electrons and ions of order 7–8 for a pure D plasma). Their exact value can be derived for example by PIC models [44]. The list of *known* model parameters for which plausible predictions or robust scalings exist is not extensive and, to improve the model's credibility, the modeller usually seeks guidance from the experiment to identify those parameters for which no first-principles model exists.

With the possibility to eliminate carbon from the model the modeller is enabled to remove one large unknown: the amount of amorphous carbon eroded from the walls and the migration of carbon material to remote places, i.e. the localization of the carbon particle source, parametrized by inhomogeneous chemical erosion/deposition parameters. As a consequence this allows to (at least partially) neglect carbon transport and carbon induced radiation in general. Historically, it has been shown that the impact of carbon can be minimized by essentially switching off the chemical erosion process in helium plasmas. In the assessment of detachment in JET-C He-plasmas it has been shown [45] that the density

Please cite this article as: S. Wiesen et al., Plasma edge and plasma-wall interaction modelling: Lessons learned from metallic devices, Nuclear Materials and Energy (2017), http://dx.doi.org/10.1016/j.nme.2017.03.033

limit seen in case of He is increased compared to D (and occurs even after the formation of an X-point MARFE in He). Power detachment in He-plasmas occurs at a lower density than particle detachment, an effect which has been reproduced by SOLPS simulations, e.g. [46]. In such modelling investigations the quantification of C-source could be neglected and the relevant processes could be easier identified which led to the actual understanding of the experimental observations (c.f. [46] for details). Of course, the consequence of a missing efficient intrinsic radiator is that another impurity radiating species is required to allow further power flux reduction towards the PFCs and the extrinsic impurity's transport characteristics must be assessed, for which however the source is known.

It should be noted that 3D edge plasma models do also exist which can be employed for the case when the 2D picture above of power and particle exhaust breaks. Fluid-kinetic 3D models like the EMC3-EIRENE code [47–49] are specifically needed if resonant magnetic perturbation coils (RMPs) are in place as it is planned for example for ITER. However, such codes like EMC3-EIRENE have their own additional limitations compared to the 2D codes and the validation process of the 3D codes has only begun as their development progresses at the same time. Nevertheless, all following conclusions about model improvements in absence of carbon using 2D codes are generally valid also for 3D codes.

3. Recovery of power fall-off length and dissipation scalings

From multi-machine regression analysis [50,51] a robust scaling expression has been derived for the power fall-off parameter λ_q representing the power flux density $q_{||}^{max} \sim P/R\lambda_q$ close to the separatrix at the outer-midplane location. So far, no size dependence on the major radius R was found but an inverse proportionality with the poloidal magnetic field strength B_p (or I_p). Scalings for λ_q have been derived from L- and H-mode discharges for low-density (attached) conditions assuming negligible volumetric power losses. A high level of regression confidence could be gained by covering JET, AUG, MAST, C-mod, DIII-D and from this it has been followed that the same scalings hold for both carbon and metallic devices.

A leading theory to explain the simple λ_q-scaling is the so called heuristic drift model (HD model) proposed in [52] which suggests that the width power flux tube is essentially a result of balancing Pfirsch–Schlueter flows against particles losses from the plasma core driven by vertical magnetic drifts (grad-p and curvature drift) and parallel losses along the field towards the divertor plates. Consistent with experiments and within the simple flow picture one can estimate a minimum density width $\lambda_n \approx 2(a/R)\ \rho_p$ with ρ_p being the poloidal ion gyro radius. The model furthermore assumes that the region with width λ_n is filled with energy by anomalous electron thermal conduction from the core which is balanced by parallel Spitzer thermal conduction. From this one concludes then that $\lambda_q^{HD} \approx \lambda_n$. The HD model fits excellently into the scaling database from Eich et al. [50].

In standard edge plasma codes like SOLPS-ITER no physics based anomalous transport model exists. Instead average values for the diffusive transport parameters $D_\perp$ and $\chi_\perp$ or pinch-velocities $V_\perp$ have to be adjusted to mimic the radial anomalous transport within the SOL. With the λ_q -scaling at hand a modeller can restrict at least in cases with lowish density the upstream transport parameters to a plausible level even without having a first principles model implemented and irrespectively from the chosen wall material. A purely laminar-drift approach (HD model) with near to zero diffusion is currently benchmarked using SOLPS-ITER [53].

Target heat flux profiles q(s) along the target are usually measured by means of infrared thermography and/or Langmuir probes [54] and a unique parametrization exists which consists of a convolution of an exponential decay (with decay parameter λ_q) with a Gaussian function representing the spreading of heat in the divertor, SOL and private-flux region (PFR) [50]. The integral power decay length [55] is defined ad $\lambda_{int} = \int(q(s)\text{-}q_{BG})ds\ /\ q_{max}$ which is well approximated by the simplified expression $\lambda_{int} \approx \lambda_q + 1.64\ S$ [56]. S is the so called diffusive power spreading parameter [57]. A complementary database of the parameter S has been collected and analysed from AUG and JET outer target IR measurements for L-mode and H-mode discharges [58]. These S parameter scalings include data from AUG and JET with carbon wall, as well as for AUG with the full-W wall, varying also the divertor configurations (horizontal and vertical target). Accompanying SOLPS modelling [58] reproduced similar S parameter scalings for both, L- and H-mode, and for varying divertor configurations. The modelling also supports the experimentally observed fact that there is no deviation from the scalings if carbon is removed from the system (i.e. in the model by switching off C sputtering and replacing the missing C radiation by D radiation with increased gas-flux). The model has eventually resulted in a robust reciprocal dependence on the target electron temperature $T_{e,targ}$ as the best ordering parameter for the S-scaling, i.e. $S \sim 1/T_{e,targ}$, for all simulation cases, a dependence which was derived with a high level of confidence (c.f. Fig. 2). The drop in T and thus increase in S can be either induced by radiation, 2D nature of heat transport (radially anomalous vs. parallel conductive) or interaction with neutrals. As observed in the experiments, for the same $T_{e,targ}$, the SOLPS model gives the same S (but not necessarily the same λ_{int} as λ_q may vary). The fact that a simple dependence for $S(T_{e,targ})$ could be derived for all the analysed data (JET and AUG, H- and L-mode, with and without C as well as varying divertor configuration) reflects the fact that an increase in S is a pure consequence of the way how T_e is reduced along the field in the SOL and hence, the scaling for the power spreading parameter S depends only indirectly on the wall material.

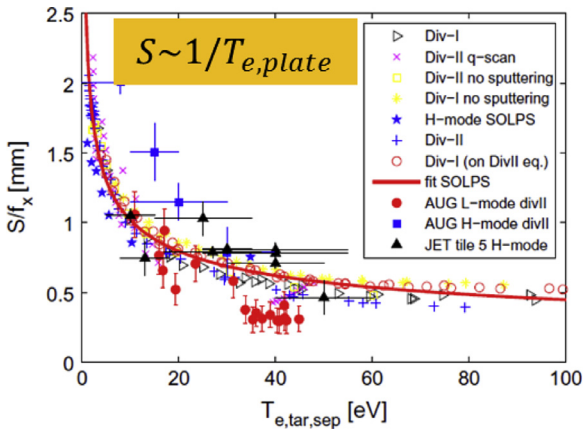

Fig. 2. Dependence of the diffusive dissipation parameter S on target temperature (reproduced from [58]).

4. Modelling power dissipation with radiation

From the λ_q-scaling the upstream parallel power flux density $q_{||}$ in ITER will be approximately 5 GW/m^2 and in the demonstration power plant DEMO $q_{||}$ will exceed 30 GW/m^2. The unmitigated perpendicular power flux density at the target plates is estimated to be 50 MW/m^2 and 300 MW/m^2, respectively [5], which would clearly exceed the tolerable material limit of 5–10 MW/m^2 (using W as actively cooled armour PFC material). Reliable power dissipation mechanisms are required to dissipate a major fraction of the total loss power P_{SOL}. In metallic devices the lack of carbon has the consequence that the missing intrinsic radiator must be replaced

Please cite this article as: S. Wiesen et al., Plasma edge and plasma-wall interaction modelling: Lessons learned from metallic devices, Nuclear Materials and Energy (2017), http://dx.doi.org/10.1016/j.nme.2017.03.033

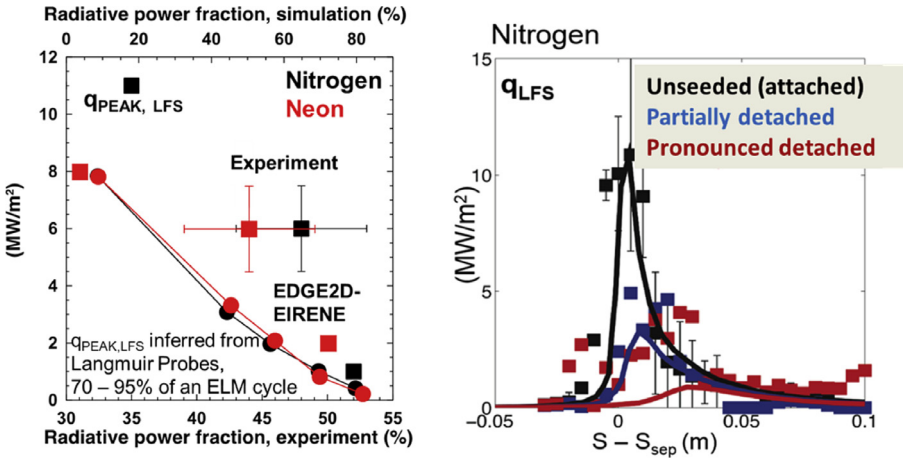

Fig. 3. Left: comparison of peak heat flux arriving at the JET LFS EDGE2D-EIRENE vs. experiment, comparing neon vs. nitrogen seeding. Right: transition from attached into pronounced detached regime for nitrogen seeding.

by an externally applied low-Z (N, Ne) or medium-Z (e.g. Ar, Kr) impurity seeding species in order to achieve heat load mitigation via radiation losses and also control of high-Z material sputtering. With intrinsic C missing also in ITER and DEMO externally puffed impurities (N, Ne, for DEMO also Ar or Kr) are essential to impose a strongly radiating regime with for significant radiation losses, i.e. radiative fractions $f_{rad} = P_{SOL\text{-}edge}/P_{rad}$, of about 60% in ITER and exceeding 95% in DEMO.

JET and AUG can be operated also in a stable pronounced detachment regime with significant X-point radiation and large radiative fraction f_{rad}. In such a strongly dissipative operational regime a record power density of about $P_{heat}/R \sim 14$ was achieved in AUG [59] (compare: ITER or DEMO will require $P_{heat}/R \sim 20$ or higher). In JET-ILW a radiative fraction $f_{rad} = 70–75\%$ at a maximum power density $P_{heat}/R \sim 9$ could be achieved with nitrogen seeding [60]. Complete divertor detachment at both targets has been observed concomitantly with strong X-point radiation. Similarly, AUG reaches a radiative fraction up to $f_{rad} \sim 90–95\%$, a larger value compared to JET which is partly related to the larger W concentration in AUG due to the W main chamber wall. A source of experimental uncertainty are errors in the analysis of radiated power, plasma loading on the limiters, errors in additional heating inputs or unobserved localised losses e.g. fast particle losses. A recent analysis of the energy balance on JET has been undertaken in [61] showing that the mismatch can be of order 20%. In order to predict the dissipation performance of a next step fusion device the existing modelling tools need to prove that they can reproduce the full transient leading into detachment. The validation process must always be seen in view of the occurring experimental uncertainties.

Nitrogen and Neon seeded JET H-mode discharges [62] have been analysed with EDGE2D-EIRENE [63] and reproduced qualitatively the transition from an attached regime to partial detachment induced by impurity radiation. With the increase in the radiative power P_{rad} a 5–10 times reduction in the peak target heat load at the LFS $q_{peak,LFS}$ has been obtained with both, Ne or N seeding. Compared to the experiment the radiation loss is underestimated by up to a factor 2 (c.f. Fig. 3). In these JET plasmas a radiated fraction f_{rad} ~50–55% has been reached experimentally. The code results also into numerically stable pronounced detachment regimes at a higher level of f_{rad}, i.e. towards similar values observed at JET achieving a maximum $f_{rad} \sim 70–75\%$ with complete LFS detachment [5]. The code does also reproduce the experimental radiation patterns. From the model neon is suggested to be a factor 5–10 stronger mantle radiator and radiates in the SOL as well as close to the pedestal. Nitrogen on the other hand radiates mainly in the divertor. Non-coronal effects [28,64] in the edge simulations is included and lead to an enhancement of radiation by broadening of radiative power function $L_z(Te)$ for a given impurity species (c.f. Fig. 4). Therefore N radiates efficiently in a broader temperature range 10–30 eV and Ne 20–150 eV, explaining the large difference in the radiation patterns observed.

A detailed analysis of the H-mode detachment transition has been pursued for AUG N-seeded discharges [65,66]. First with increasing density (and with no seeding) the onset of detachment is observed a the HFS divertor. As the density increases further a fluctuating regime is observed with fluctuations at the X-point. Additionally, the establishment of a HFS high-density (HFSHD) region is observed [67] which can be sustained by a significant fraction of power carried in the HFS far-SOL towards the divertor plates. With external seeding (e.g. N) LFS divertor partial detachment is triggered concomitantly occurring with strong N-radiation close to the X-point. At the same time the HFSHD region disappears. With increasing the N-seeding even further, a complete detachment regime can be established in which radiation (nitrogen and Balmer) is mainly condensed inside the confined plasma, i.e. at the X-point. The appearance of the radiation at the X-point is in parallel with a temperature loss just inside the confined region above the X-point. The strong X-point radiation triggers a loss in the pedestal pressure, i.e. a depletion of $T_{e,ped}$ and $n_{e,ped}$ potentially driven by transport along poloidal gradients into the X-point regions. Similar observations of pedestal pressure loss with impurity have also been observed in JET [60].

SOLPS modelling is able to reproduce the attached and completely detached states in seeded H-mode. The standard procedure is to fix for a given level of density the upstream and downstream diffusive transport to values which allows to match plasma profiles measured by Li-beam, Thomson-scattering and CXRS measurements (upstream, c.f. Fig. 6) and at the same time target profiles measured by Langmuir probes and IR tomography. The full path of particles and radiation disconnecting from the targets in a partial detached regime until complete detachment with condensation of density and radiation close to the X-point can be reproduced with the code [68] (c.f. Fig. 5). An essential ingredient in the model is the inclusion of cross-field drifts to ensure in/out asymmetries. Although the transition into detachment can be understood some caveats still exist in this approach as some generic quantities could not be matched. For example in the complete detached state the fuelling and seeding rates assumed in the model are too low compared to the experiment (factor 5–8) and consequently the neutral

Please cite this article as: S. Wiesen et al., Plasma edge and plasma-wall interaction modelling: Lessons learned from metallic devices, Nuclear Materials and Energy (2017), http://dx.doi.org/10.1016/j.nme.2017.03.033

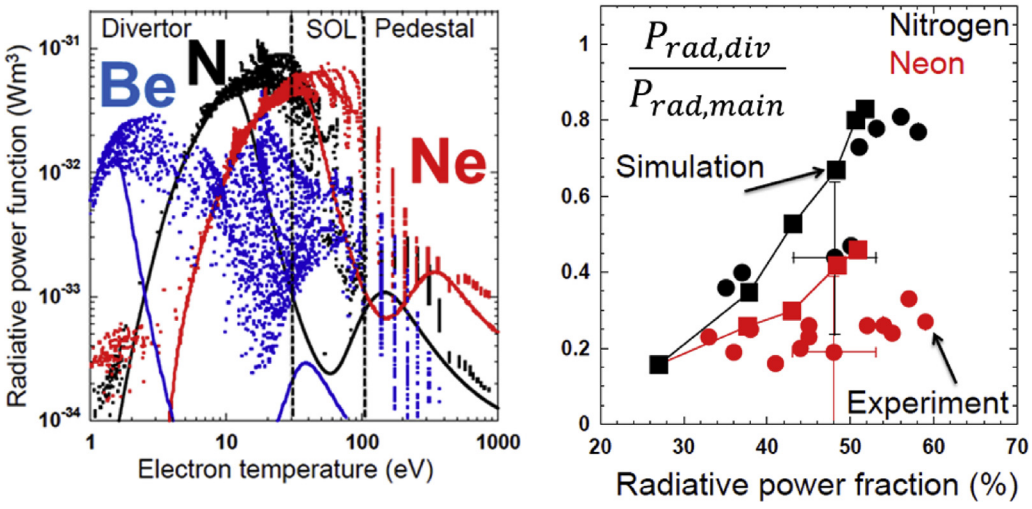

Fig. 4. Left: Radiative power function $L_z(T_e)$ for Be, N and Ne. solid line: coronal approximation, dots: non-coronal approximation (including transport from EDGE2D-EIRENE JET simulations [63]), Right: ratio of radiated power in JET divertor vs. main chamber.

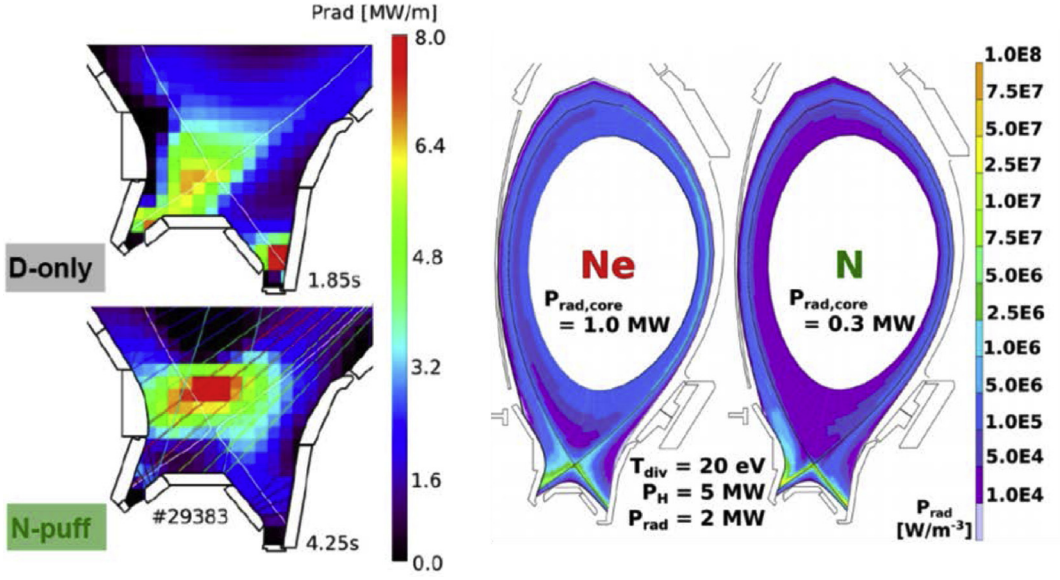

Fig. 5. Comparison of AUG radiation profiles from experiment (left) vs. SOLPS5 (right) (reproduced from [68]).

pressure is too low (factor 2–6). In order to match the downstream profiles an increase of radial transport in the divertor was necessary (factor 3) and additionally a separate rescaling for the HFS/LFS transport was necessary. With this caveat, still, SOLPS is able to recover also the upstream to downstream pressure loss mechanism for the outer target within a factor 1.6 (c.f. Fig. 6).

With this result it seems that one must accept that the validation of a code like SOLPS is hampered as for each modelled plasma a separate scaling of the transport is necessary to match up- and downstream profiles. The trend to increase the transport at higher density has led to parameterisations of anomalous transport for example by scaling it with plasma parameters like collisionality or density [26]. This rescaling method using feedback on the plasma solution helped in terms of allowing a particle flux roll-over at lower density (i.e. closer to the experimentally observed value) but did also lead to numerical oscillations in the completely detached case. It has only been recently reported [67] that a tremendous improvement could be achieved in terms of transport prescription making a rescaling in the divertor unnecessary. By assuming an extra advective transport loss channel for transverse transport in the SOL and at the same time reducing the pedestal transport it is possible to reproduce the full cycle of detachment including the establishment of the HFSHD region without rescaling of diffusive transport in the divertor. Still, a model for cross-field drifts needs to be included to reproduce the in/out asymmetries + HFSHD. The deficiency to underestimate the required fuelling as well as a too low divertor pressure has been effectively eliminated, however only for a single kind of AUG discharge. It turns out, that one critical ingredient for a validated edge model is to match the neutral pressure in the divertor

5. Neutral transport and divertor compression and impact on power exhaust modelling

In metallic devices the way the plasma is recycled at the PFCs has changed significantly. With no C present on the recycling surface the particle source by chemical erosion has been effectively switched off causing the particle influx essentially to be given by the total particle throughput Φ. Hence transport has at least to some extent become more important to define the particle content

Please cite this article as: S. Wiesen et al., Plasma edge and plasma-wall interaction modelling: Lessons learned from metallic devices, Nuclear Materials and Energy (2017), http://dx.doi.org/10.1016/j.nme.2017.03.033

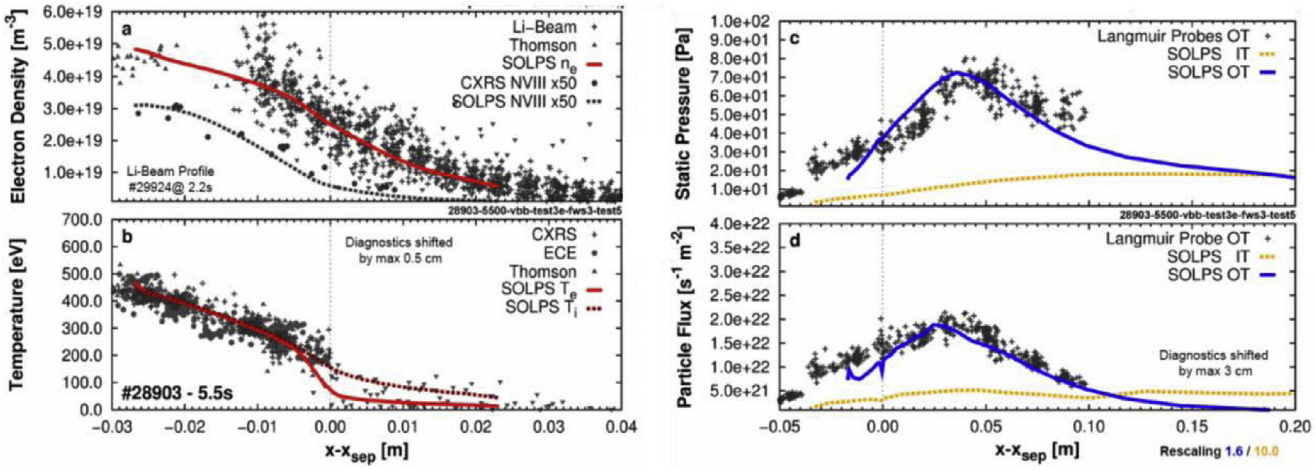

Fig. 6. Left: upstream n_e and T_e for similar AUG N-seeded discharges (symbols) vs. SOLPS (solid line). Right: downstream pressure and particle flux at inner (IT) and outer (OT) target, (reproduced from [68]).

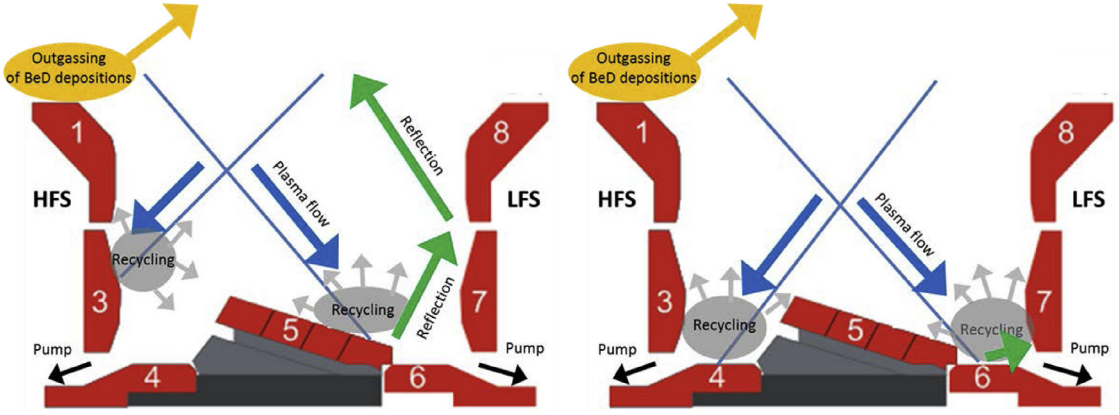

Fig. 7. Schematic comparison of vertical (VT) and horizontal (HT) target configuration in JET-ILW and neutral recycling sources and ballistic trajectories. The outgassing of D particle on top of the HFS baffle occurs during an ELM and has been measured by fast cameras [87].

as pumping and fuelling is less affected by the wall. On the other hand, metal PFCs are also able to sustain specific kinetic transport effects, e.g. competitions between slow moving particles being reemitted from the surface as recycling neutrals and fast ballistic neutrals from charge-exchange processes or surface reflections (c.f. Fig. 7). This can have consequences on the core plasma fuelling [19] which was also supported by EDGE2D-EIRENE simulations for seeded JET H-mode discharges [18]. In these simulations the radiation fraction has been increased by N-seeding and the influx of fuel particles had been compared between (semi-) horizontal (HT) and vertical target (VT) configurations. At large radiative fractions f_{rad}, and hence with an overall cooler divertor, the influx of D atoms from LFS in HT is a factor 6 stronger than in VT, whereas at lower f_{rad} both VT and HT behave similar in terms of core fuelling (c.f. Fig. 8). This effect cannot be related only to the pedestal pressure loss at high f_{rad} as pressure loss occurs in both VT and HT configurations in similar ways. Rather the drastic change of the LFS fuelling in HT must be related to the qualitative change of neutral transport, i.e. fast neutral particles fuelling more efficiently the LFS in HT.

In metal devices the divertor configuration itself and neutral kinetics thus may have a stronger impact on the neutral distribution in the volume and thus the level of neutral compression in the divertor. Hence it is mandatory to model the neutral distribution correctly including the geometric details and to validate the neutral model for example against pressure gauge measurements. The difficulty in modelling neutral compression has been highlighted by the model-based radiation scalings which had been derived for N-seeded JET-ILW and AUG discharges in L-mode using the SOLPS5.0 code [69]. The model was quite successful in identifying three radiative regimes which are in line with the experimentally observed data: 1) a low radiating regime ($f_{rad} \sim$ 5–10%) with most of the radiation located in the inner divertor, 2) a regime with maximum level of radiation in the divertor up to $f_{rad} \sim$ 60%, and 3) maximum total radiation with the radiation front moving above the X-point i.e. into the confined region (c.f. Fig. 9). The model does also reproduce well the experimentally observed radiative asymmetry in the divertor legs if cross-field drifts (ExB and grad-B) are included. The model recovers qualitatively well the empirical scaling law for divertor radiation with increasing N2 injection taken from [70], i.e. $P_{rad,div} \sim p_{0,div}^{0.5} R_0 \lambda_q (Z_{eff}-1)^{0.3}$ with $p_{0,div}$ the neutral pressure in the divertor. However the scaling underestimates the modelled JET-ILW data by a factor 0.4 whilst the match with AUG is better and within a factor 1.2 (c.f. Fig. 9). This discrepancy could be partly related to the fact that, contrary to AUG, the modelled JET discharges were in semi-horizontal divertor configurations with the LFS strike-point located on the horizontal target and thus stronger pump action of neutral impurities into the LFS corner pump throat is expected [71], the latter however was not fully included in the SOLPS model as the neutral conductance towards the cryo-pump was mocked up in the code by specifying fixed pumping albedos in the divertor corners. More likely however are uncertainties in the experimental data for Z_{eff} or $p_{0,div}$ (these quantities are taken for examples from different locations in JET and AUG whereas in

Please cite this article as: S. Wiesen et al., Plasma edge and plasma-wall interaction modelling: Lessons learned from metallic devices, Nuclear Materials and Energy (2017), http://dx.doi.org/10.1016/j.nme.2017.03.033

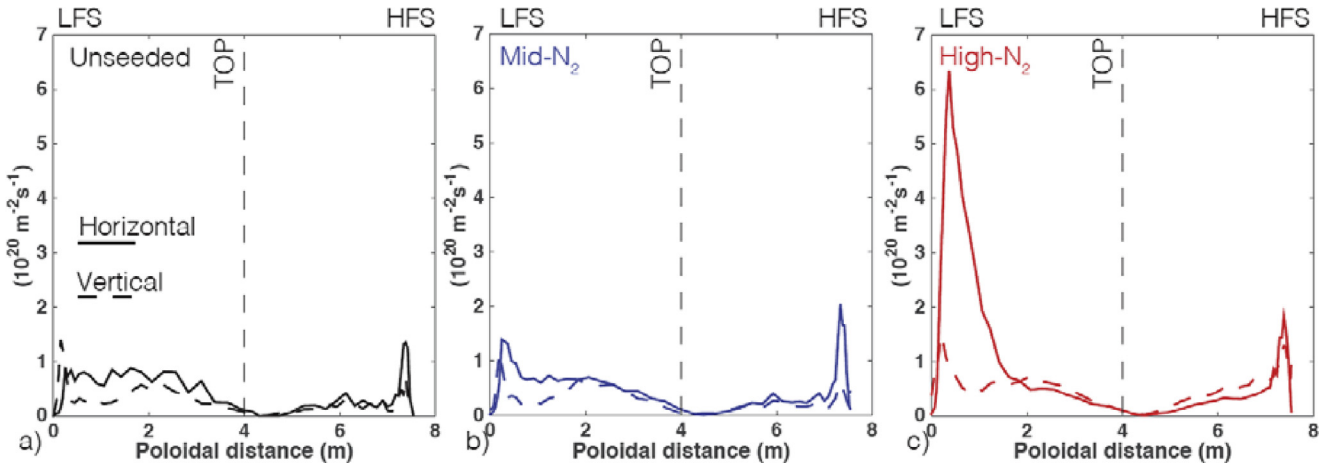

Fig. 8. EDGE2D-EIRENE sensitivity studies of poloidal fuelling profiles for varying JET divertor configurations, from left to right: increasing N2 seeding (i.e. radiative power) (reproduced from [18]).

the model identical diagnostics for these scaling parameters had been used) or in the assumptions on the upstream λ_q in the model [69] vs. scaling [70]. Furthermore it is difficult in JET, contrarily to AUG, to measure $p_{0,div}$ as there is no good coverage with pressure gauges. Hence, $p_{0,div}$ has been identified as one of the crucial parameters which correlate well with the evolution of the total radiated power with increasing seeding level. Therefore it is important that we can trust the modelled values and have correct, i.e. validated, models for the neutrals.

The impact of the spatial neutral distribution on detachment has been analysed in greater detail for JET-ILW unseeded L-mode discharges for (semi-) horizontal (HT) and vertical target (VT) configurations using the EDGE2D-EIRENE code package [72]. Here the transport in EDGE2D was purely diffusive and fixed for all densities but cross-field drift were included. The result was that with increasing LFS upstream density $n_{e,sep}$ the calculated roll-over of the LFS and HFS plate-integrated ion currents $I_{div,HFS}$ and $I_{div,LFS}$, respectively, occurs close to the same $n_{e,sep}$, slightly shifted to 10–15% lower $n_{e,sep}$ in VT than in HT configuration. This is consistent with the experimental data (c.f. Fig. 10). However, the behaviour of the estimated LFS peak plate temperature $T_{e,pk,LFS}$ is not: $T_{e,pk,LFS}$ drops down below 2 eV at 30% lower $n_{e,sep}$ in VT than in HT configuration, a result not seen in the experiment. This discrepancy could not be fixed by switching on cross-field drifts in EDGE2D-EIRENE as this was resulting in dropping the $T_{e,pk,HFS,}$ but kept $T_{e,pk,LFS}$ similarly low as in the case without drifts. A model to mimic a by-pass leak at the tile gap of the LFS vertical target plate also did not raise $T_{e,pk,LFS}$ either as the neutral density in front of the tile gap is too small to impact the overall recycling at the LFS plate.

Also in [72] a deeper analysis of the neutral fluxes towards the pump throats revealed that 80% of the total injected deuterium has been pumped at the LFS in HT whereas in VT it was only 30% (assuming equal pumping speeds or albedos at the pumping corner surfaces). This was unexpected as with consideration of the neutral conductance and shorter path lengths of the neutrals reaching the cryopump in JET at the LFS, the LFS pump should be more efficient. Indeed, the simulations indicate that neutrals which have to travel through the PFR to reach the LFS pump could compete well with the reflected ballistic neutrals from the metallic plates in HT into the LFS pump throat. However, it was evident that the total amount of neutral pumping (i.e. the particle throughput) Φ_D was approximately a factor 3 lower compared to the experiment to reach the detachment roll-over. As an additional difficulty the neutral divertor pressure $p_{0,div}$ could not be benchmarked as the only available pressure gauge in JET is located 2 m below the divertor baseplate, in the lower part of the so-called sub-divertor region.

A subsequent improvement of the neutral model in EDGE2D-EIRENE includes an extension of the neutral EIRENE simulation grid into the sub-divertor region [73] that was capable to include the neutral conductance towards the cryopump, leakages around the divertor as well as the location of the sub-divertor pressure gauge. In [73] the same discharges as in [72] have been analysed again and a clear linear relationship between the throughput Φ_D and the measured $p_{0,sub-div}$ was found, i.e. $\Phi_D/p_{0,sub-div} = const$, that agrees well with the experiment (c.f. Fig. 11). The required experimental value of Φ_D was a factor 2–3 higher in VT than in HT to reach a given upstream density $n_{e,sep}$, a result reproduced by the extended EDGE2D-EIRENE model including the sub-divertor model within a factor of 2. At lower $n_{e,sep}$ the pumping is more balanced in VT compared to HT, albeit this is not the cause for a higher Φ_D required in VT. It is rather the number of neutral particles capable to penetrate the separatrix being smaller in case of VT, requiring a larger Φ_D to reach a given $n_{e,sep}$, i.e. requiring a greater particle content. At higher $n_{e,sep}$ the situation is different: for a given Φ_D the neutral penetration across the separatrix is similar in HT and VT but the pumping is increased in VT due to particles reaching the cryopump either below the PFR plasma or circumventing the plasma by recirculation of neutrals leaving the LFS pump throat reaching the cryopump through the sub-divertor structures (c.f. also the benchmark work using the DSMC code DIVGAS [74,75]). From the model linear dependencies for the neutral pressures at the LFS and HFS pump throat, $p_{0,div-LFS}$ and $p_{0,div-HFS}$ respectively, are derived as function of $p_{0,sub-div}$ (c.f. Fig. 11): in VT $p_{0,div-LFS} \approx p_{0,div-HFS} \approx 6\ p_{0,sub-div}$ and in HT $p_{0,div-LFS} \approx 6\ p_{0,sub-div}$ and $p_{0,div,HFS} \approx 4\ p_{0,sub-div}$. These factors are however only valid for the considered unseeded L-mode density scan. Reviewing the model-based scaling attempt from [69] described previously and with the assumption that $p_{0,sub-div}$ instead of $p_{0,div-LFS}$ has been assumed in the reproduction of the scaling of $P_{rad,div} \sim p_{0,div}{}^{0.5} R_0 \lambda_q (Z_{eff}-1)^{0.3}$ the missing factor 0.4 for JET-ILW in [69] could be recovered by the mismatch between $p_{0,sub-div}$ and $p_{0,div-LFS}$, i.e. 1/sqrt(6). However it needs to be stressed again, that still other uncertainties for example in Z_{eff} or λ_q cannot be ruled out as a cause for discrepancies between radiation scaling and experimental data.

A quantitative assessment of the dominant atomic and molecular processes governing the neutral dynamics has been discussed in [76] using the OSM-EIRENE interpretative model for Alcator C-mod. C-mod, having a small major radius of 0.65 m, can be

Please cite this article as: S. Wiesen et al., Plasma edge and plasma-wall interaction modelling: Lessons learned from metallic devices, Nuclear Materials and Energy (2017), http://dx.doi.org/10.1016/j.nme.2017.03.033

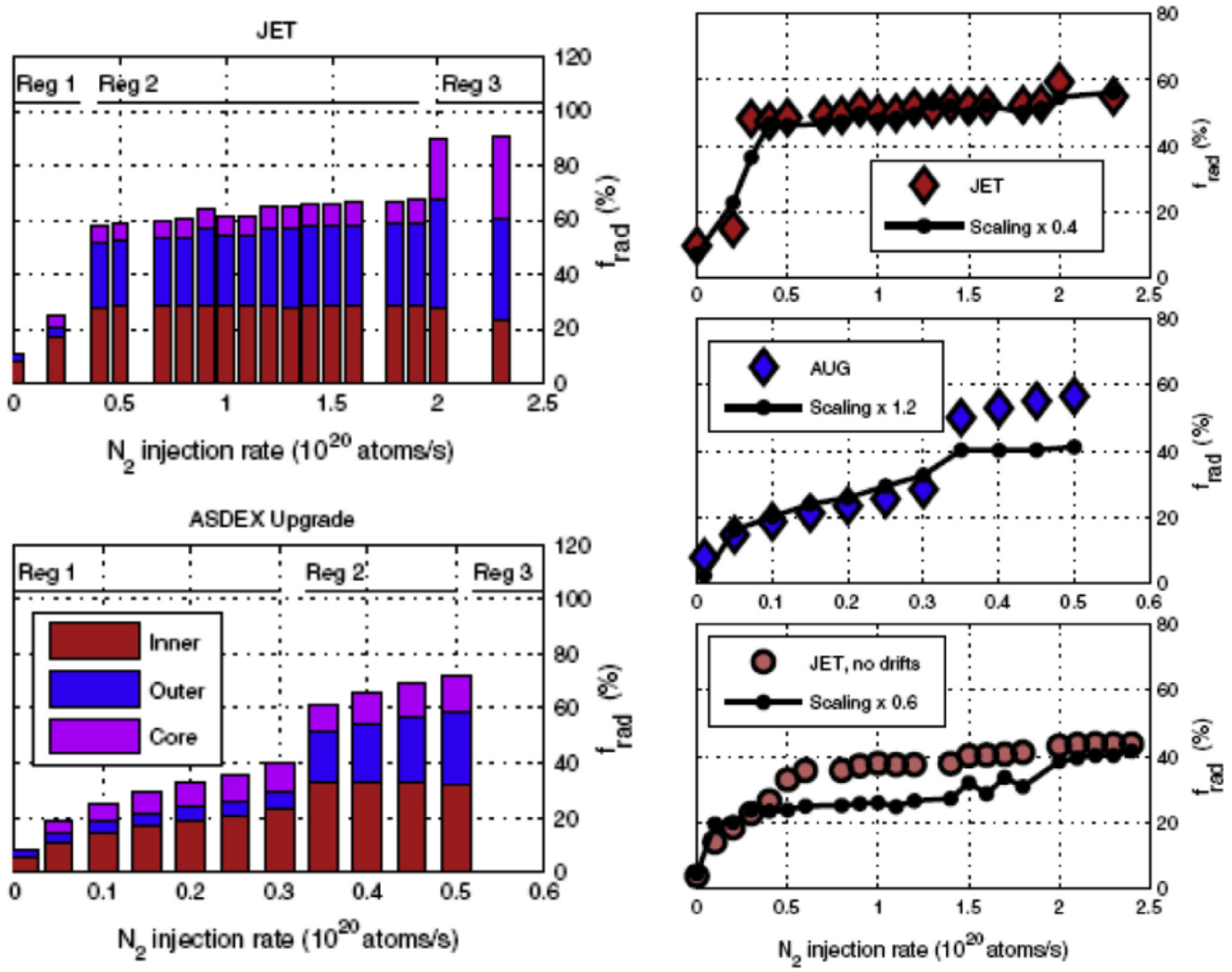

Fig. 9. Left: comparison of the 3 radiative regimes in JET and AUG L-mode discharges calculated with the SOLPS5 code. Right: comparison with empirical scaling law $P_{rad,div} \sim p_{0,div}^{0.5} R_0 \lambda_q (Z_{eff}-1)^{0.3}$ from [70] (reproduced from [69]).

regarded as relevant for ITER in the sense that the average density is higher than in other devices and thus C-mod has "ITER-like" features (vertical divertor targets and large neutral pressures) which allows to validate the physics model relevant for ITER conditions. In order to match the neutral pressure and Balmer radiation profiles within a factor of 2 using OSM-EIRENE the following processes had to be included: Ly-α opacity, neutral viscosity, molecular assisted recombination (MAR) as well as ion-molecule elastic collisions. All these processes had been included in the ITER design studies [77,25] and in principle all those processes can be included in all edge codes with coupling to EIRENE. Recently, it has been reported that a radiation short-fall was recovered in the modelling of unseeded JET [63,72,78] or AUG [68] discharges (with metallic walls) using SOLPS or EDGE2D-EIRENE. The short-fall is characterized by a factor of 2–10 lower D_α line emission compared to spectroscopic measurements and may occur even if the neutral divertor pressure is matched to the experiment and with or without N-seeding. At high densities this could be related to missing terms in the D_2 and D_2^+ molecule dissociation [78] following emissions of electronically excited D atoms. Such terms, if significant, should be accounted for in the calculation of the emitted D_α radiation in the model and/or in the corresponding energy sink terms passed over from EIRENE to the plasma fluid code. Currently, a revision of the underlying neutral physics model is ongoing, investigating again the relevance of specific processes like fast atoms from molecular dissociation, Lyman-opacity [79-80] or the impact of vibrationally excited recycling molecules and MAR enhancement [81], exploiting revised and cross-calibrated spectroscopic measurements at JET. So far, the issue of D-radiation short-fall is still an unresolved issue.

Recent simulations for Alcator C-mod [82] using the new SOLPS-ITER code [31] employing an EIRENE model as suggested in [25] (which does not take into account Lyman-opacity or neutral viscosity effects) support the fact that adding neutral leakage paths in the model is indeed essential for the correct modelling of divertor conditions, specifically for the case of high density. The C-mod plenum pressure is very sensitive to the level of geometric details included. The impact on the plasmas solution itself is not sensitive to details of the actual leakage path however the sole existence of leakage paths has a strong impact on the neutral pressure and thus on the plasma solution (i.e. no leakage into the C-mod plenum leads to a too cold divertor plasma). With the inclusion of leakages and adding also cross-field drifts at the same time into the SOLPS-ITER model an excellent agreement for the upstream profiles could be achieved (in both, forward and reversed field configurations). The LFS target profiles match also excellently with the Langmuir probe data and $T_{e,plate}$ asymmetries are reproduced. However, the transition into HFS detachment remains elusive. It is hoped that also this last discrepancy can be resolved by improving the

Please cite this article as: S. Wiesen et al., Plasma edge and plasma-wall interaction modelling: Lessons learned from metallic devices, Nuclear Materials and Energy (2017), http://dx.doi.org/10.1016/j.nme.2017.03.033

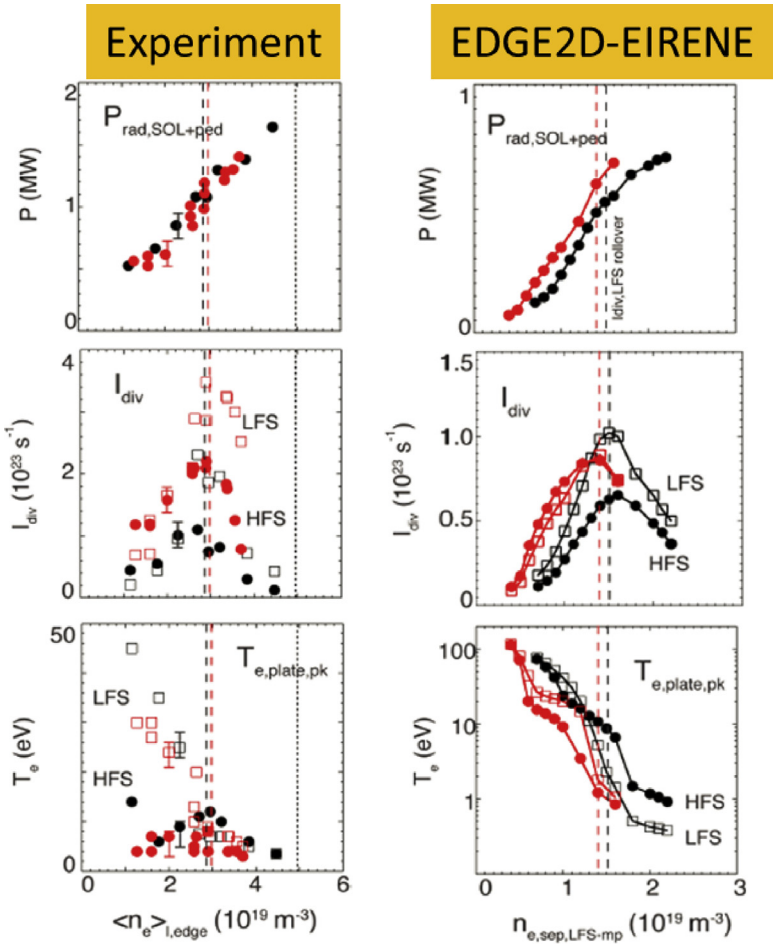

Fig. 10. Comparison of transition into detachment as function of upstream density n_e: EDGE2D-EIRENE vs. JET L-mode discharge (unseeded). From top to bottom: total radiated power, total saturation current, plate temperature. Black symbols horizontal target (HT), red symbols vertical target (VT) configuration, Open symbols LFS, closed symbols HFS. (For interpretation of the references to colour in this figure legend, the reader is referred to the web version of this article.)

transport model of the plasma, e.g. assuming an advective component for the anomalous transport as suggested in [67].

6. Integrated PWI modelling

With increasing density, particle losses in radial direction towards the main-chamber increase. When approaching divertor detachment the particle flux rolls over at the target plates and the global particle flow pattern must account for this by enhanced transport perpendicular to the field for plasma and neutral particles (only part of the global particle loss is accounted by volume recombination). Li-beam measurements at AUG and JET have shown that with the increase of the Greenwald fraction f_{GW} the radial density profile flattens [83]. Also a formation of density shoulder has been observed with increase of density which can be linked with the actual divertor geometry of the discharge (depending to the closure of the divertor ballistic effects in neutral transport, c.f. [84]). The increase of perpendicular flux with density has been observed also in COMPASS [83], DIII-D and C-mod [85], TCV [86], KSTAR [87]. The increase of radial plasma transport with collisionality has also been recovered regularly by simulations ([88,89] and references therein) highlighting the role of interchange instability driven turbulence.

With the increase of flux towards the main-chamber walls effects from plasma-wall and neutral-wall interaction like material erosion become more relevant. Specifically, the assessment of Be erosion, migration and particle retention in Be co-deposited layers has become an important issue for ITER [8]. A detailed investigation to assess the amount of Be produced and transported to remote areas leading to co-deposition, fuel retention and also dust formation is required. An integrated approach is thus necessary for bringing together the dependencies of the flux arriving at the first wall and the actual PWI processes involved. Historically, standard edge tools like EDGE2D-EIRENE or SOLPS have not taken into account the direct interaction of the plasma with the main-chamber wall as the simulation grid was not in direct touch with the walls surfaces. Recent developments however in the code SOLEDGE2D-EIRENE has led to the implementation of a so called wide-grid extension of the simulation grid up towards the first wall [35]. Similar code extensions are currently also in preparation for the SOLPS-ITER code package. Without the extension of the grid, the codes assume that the plasma decays with a fixed decay length at the grid boundary. Only the EIRENE neutrals in any of the aforementioned codes could interact with the first wall and the exposure of PFCs to energetic CX neutrals were already discussed in the past. With no grid extension to the wall however the plasma particle fluxes measured with Langmuir probes could not be matched [90] and consequently the calculation of erosion fluxes and global impurity yield depended strongly on the assumed boundary conditions (ideally a 3D model to be used for this to take into account also recessed areas and components in the vessel). Combined OSM-EIRENE/DIVIMP simulations with no grid extension estimated a variation of Be erosion fluxes within at least one order of magnitude [91]. Now with a grid extension included the flux towards the wall is a function of

Please cite this article as: S. Wiesen et al., Plasma edge and plasma-wall interaction modelling: Lessons learned from metallic devices, Nuclear Materials and Energy (2017), http://dx.doi.org/10.1016/j.nme.2017.03.033

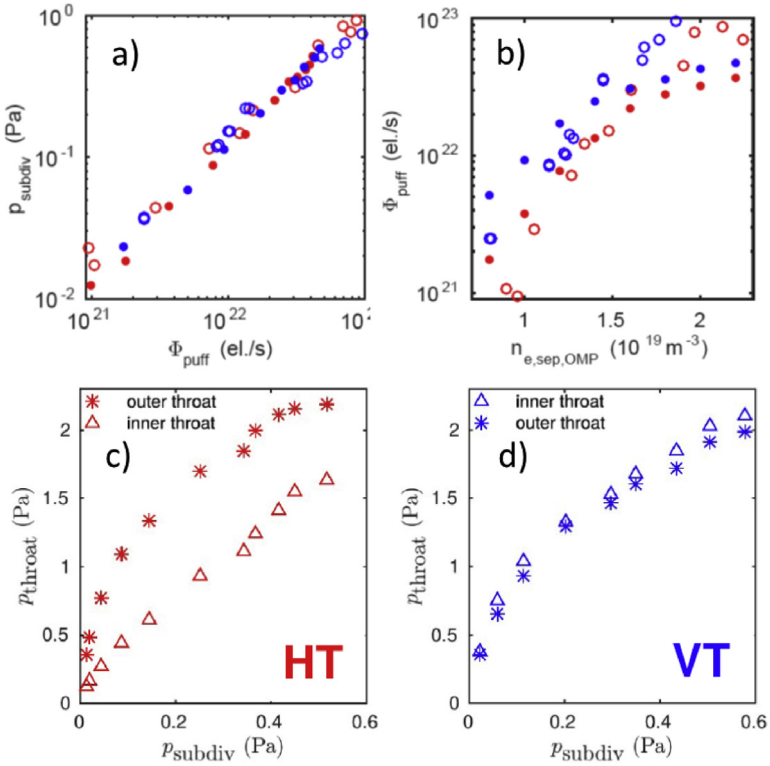

Fig. 11. a) JET subdivertor pressure $p_{sub,div}$ as function of throughput Φ_{puff} in experiment (open circles) and simulation (solid circles) and in HT (red) and VT (blue) configurations. b) Φ_{puff} as function of $n_{e,sep,OMP}$, symbols as in a). c) pressure p_{throat} in divertor corners vs. sub-divertor pressure $p_{sub,div}$. (reproduced from [73]). (For interpretation of the references to colour in this figure legend, the reader is referred to the web version of this article.)

the overall plasma solution and the assumed anomalous transport model and the free decay length input parameter can be replaced by a proper sheath physics model at the wall. SOLEDGE2D-EIRENE has included an improved model for the plasma sheath boundary conditions for the case of glancing angles [43]. First simulations for JET-ILW L-mode discharges showed that additional erosion zones near the top-plane and at the LFS first wall could be recovered and thus led to the observation of a rather inhomogeneous Be-erosion pattern [35].

Recently, the Be erosion process has been thoroughly assessed by molecular dynamics (MD) codes in greater detail. It was found that in addition to the physical sputtering process a chemically assisted sputtering channel producing BeD_x molecular compounds has been identified numerically [92] and also experimentally [93]. The BeD sputtering process requires a finite level for the projectile impact energy E_{D+} and increases with E_{D+}. Recent MD simulations have also shown that a dependence of the surface baseplate temperature T_{base} exists too, i.e. a decrease of the BeD yield with increasing T_{base} [94]. Also this has been recovered by spectroscopic gas-balance [93] (c.f. Fig. 12) resulting in the observation that with increasing T_{base} the amount of D produced by BeD erosion can be compensated with D from dissociating D_2. A new database including the full set of Be erosion processes has been derived from the MD simulations to be used in PWI codes like ERO [12,13]. A comparison of the effective total Be erosion yield as a function of $T_e < 30$ eV calculated by ERO shows a fair agreement to the measurements within a factor 3–5 (c.f. Fig. 12). Above $T_e = 30$ eV the Be yield is strongly enhanced by Be self-sputtering.

To assess the particle fluxes and erosion patterns into remote areas in JET-C and JET-ILW a comparative study using the ERO Monte-Carlo code was done [95]. In this case the divertor plasma background parameters have been parametrized (radial density and temperature profile widths, impurity concentrations, etc.) to allow a larger flexibility in the sensitivity studies pursued. The ERO simulations reproduced the experimental result that high-Z material influx by W-sputtering is only by ELMs in H-mode discharges and that a finite level of Be is transported into remote areas due to reflections at W-PFCs. Hence, for Be migration, kinetic effects play a major role. Transport of neutral Be particles seems to be responsible for fluxes into regions below the horizontal target, not accessible by the plasma. For both, JET-C and JET-ILW, the fluxes of intrinsic low-Z impurities into remote areas are qualitatively similar. A slightly stronger dependency on the divertor geometry (strike-point location either on VT or HT) is recovered in JET-ILW due to ballistic effects. In absolute numbers the deposition rate in the model is an order of magnitude smaller compared to the derived value from the rotating collector probe [95]. This discrepancy could be relaxed by reducing the level of beryllium influx into the JET W divertor, provided as an external parameter to the ERO code (from 1% down to 0.1% of the total particle flux) and by including erosion from fast charge exchange neutrals. New shot-resolved QMB experiments at JET are under way to better quantify and validate the ERO model. The interpretation of such in-situ measurements of the local deposition rate is however complex [96].

With emerging of sophisticated databases for the Be sputtering yields plus the possibility to derive the actual particle flux arriving at the first wall with grid extensions one is in a better position to understand the global Be material migration process, transport and particle retention at the same time. The combination of the WallDYN-DIVIMP code package [97,98] has the capability to achieve this. WallDYN splits up the first wall (main-chamber and divertor) into a number of segments, each representing a PFC consisting of a near-surface reaction-zone and deeper lying bulk-zone. The information about particle fluxes (bulk plasma and/or impurities) is taken for example from a SOLEDGE-EIRENE simulation and is distributed across the set of PFC segments. The impurity

Please cite this article as: S. Wiesen et al., Plasma edge and plasma-wall interaction modelling: Lessons learned from metallic devices, Nuclear Materials and Energy (2017), http://dx.doi.org/10.1016/j.nme.2017.03.033

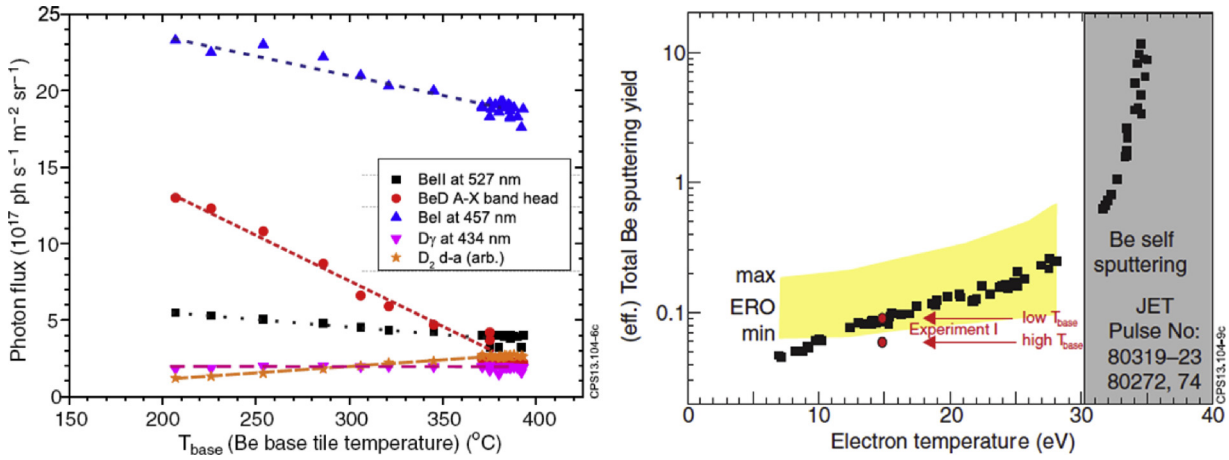

Fig. 12. Left: Photon flux evolution of the different species as function of the base temperature of the bulk Be tile 7 in JET, Right: effective Be sputtering yield as function of the local T_e. The shadowed area indicates ERO modelling. (reproduced from [93]).

Monte-Carlo code DIVIMP is then used to calculate the particle transport of the eroded particles from each segment to another. The yield coefficients for erosion and sputtering are taken from revised MD simulation databases or using TRIM data. As a result one derives a migration matrix telling how much material has been transport from each source segment to another destination segment. With this approach it was possible to confirm the experimentally observed migration and deposition pattern of Be, i.e. a net deposition zone on top of the HFS upper baffle plate on top of the JET-ILW divertor [99]. Another example is the transport of N using the WallDYN package [100]. The availability of a global migration code WallDYN-DIVIMP combined with validated extended plasma backgrounds from SOLEDGE2D-EIRENE or SOLPS-ITER is a major step forward in the field of integrated modelling predictions for ITER and DEMO. New developments to couple 3D codes (e.g. EMC3-EIRENE) with WallDYN to take into account the full 3D structure of the vessel and also perturbed magnetic field topologies are currently in preparation.

To highlight one more example for which an integrated modelling is required, is linked to pedestal physics, power exhaust and PWI physics. It has been observed in JET-ILW that compared to JET-C the pedestal density evolution is retarded after an ELM-crash. The duration it takes to build up the n_e- and T_e-pedestal after an ELM seems to be dependent on the level of recycling and varies between 1–10 ms in JET-ILW [101] and pedestal height depends also on selected divertor configuration and pumping [102]. A similar evidence for the change of the pedestal behaviour has been found also in AUG however with different time-scales for rebuilding the pedestal [19]. Time-dependent EDGE2D-EIRENE simulations of ELM dynamics for JET were not capable to explain the retarded pedestal refuelling process [103] as these assumed a fixed model for the transport in the pedestal region between the ELMs. Hence the interplay between pedestal transport and pedestal fuelling could not be consistently modelled. Full MHD models like the JOREK [104] do exist but lack the sophisticated neutral and PWI models required to consistently simulate the particle exhaust mechanism. Integrated core/edge/SOL/PWI schemes do already exist [105–109] (c.f. Fig. 13) and depending on the flavour the sub-models for core-, SOL/edge- or PWI-physics are superior or inferior to others. Two hypotheses have been put forward to address the retarded fuelling effect: a) pedestal fuelling could be impacted by dynamic reservoir effects during ELMs which stem from D particles being outgassed after implantation into traps of the W or Be wall material and co-deposits [22,110], or b) volumetric particle reservoirs may lead to a retardation of pedestal recovery between ELMs due to lagged neutral transport within the divertor (including sub-divertor structures of the vessel) [111]. To address such reservoir effects and their impact on pedestal performance the integrated code JINTRAC (a combination of the 1.5D core code JETTO with the EDGE2D-EIRENE SOL/edge code) has been modified to include finite surface reservoirs in the PFCs [112]. As a principal result it was found that indeed a reduced recycling coefficient at the PFCs after an ELM crash leads to a delay in pedestal density increase and subsequently to lower confinement due to stiff core transport. The retardation of the density built-up seen in the JINTRAC integrated model is also a strong function of the assumption of a predefined recycling coefficient R between ($R = 1$) and at the ELM ($R < 1$). As a consequence of the oversimplified pedestal transport model no direct coupling between density and temperature was included, and hence there was no delay in pedestal temperature after the ELM. To improve for this a coupling of particle and heat transport in the pedestal (e.g. [113]) in between ELMs should be implemented into JINTRAC. The integrated JINTRAC model in principle has the capability to model volumetric reservoir effects during the ELM evolution in time. In [112] no sub-divertor model was present and the time-dependency of neutrals in EIRENE was neglected. Apart from an improved pedestal model future integrated model schemes to assess fuelling during the ELM cycle should include: the full time-dependent neutral model in EIRENE, at least a 2D full sub-divertor structure model up to the cryo-pumps [73] as well as a time-dependent coupling to a trap-diffusive model for the recycling coefficient representing the outgassing effect from W- or Be-PFCs [114,115].

The previous example has highlighted what could be done with an integrated set of codes. However, progress in integrated (global) modelling is frustratingly slow as each individual sub-module has its own deficiencies which need to be resolved by separate validation activities. For the topic of particle and power exhaust this has been discussed in previous sections. Up to date, a full scenario modelling for an existing tokamak device is still pending. It needs to be stressed that a pure technical coupling of physics modules does not necessarily mean elimination of unknown model parameters (e.g. boundary conditions) as feedback mechanisms between the sub-models increase the overall non-linearity of the numerical system making an achievement of global convergence hard. In many cases the coupling is also not self-consistent (in case of coupling of a 1D core code with a 2D SOL code: what quantities should be exchanged from which location in space?) which makes the interpretation of numerical results often difficult.

Please cite this article as: S. Wiesen et al., Plasma edge and plasma-wall interaction modelling: Lessons learned from metallic devices, Nuclear Materials and Energy (2017), http://dx.doi.org/10.1016/j.nme.2017.03.033

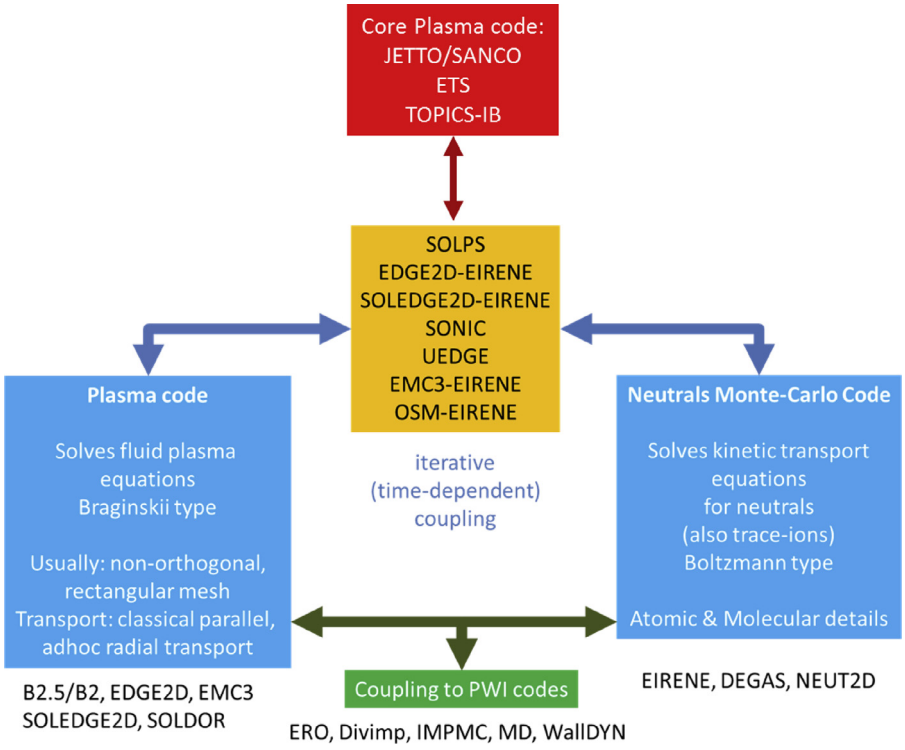

Fig. 13. Schematic diagram of integration of codes.

7. Summary and conclusions

The absence of C in metallic devices does allow a disentanglement of relevant processes in the understanding of the power and particle exhaust problem. With the absence of carbon as the primary plasma impurity and radiator it is possible to eliminate some of the free parameters for impurity transport from the models, i.e. chemical sputtering and consequences from hydro-carbon transport physics and retention in amorphous carbon layers. The particle content in metallic devices is mainly driven by the particle throughput and not by hydrocarbons created by the chemical erosion process which homogenize the plasma fuelling.

Significant progress has been made in the validation of standard modelling tools like SOLPS or EDGE2D-EIRENE to model reactor relevant dissipative (radiative) divertor regimes exploiting plasma detachment for reducing target heat loads. Somewhat robust scalings exist for the description of the upstream power decay length parameter λ_q at least in low to medium density independently of the wall material. However a general scaling for the dissipation process in the divertor does not exist as the parallel temperature drop towards the divertor plates is impacted by a manifold of physics effects: system size, divertor geometry, neutral compression, radiation loss, stiff 2D nature of transport in the SOL etc. Some machine-dependent scalings exists for the transition into detachment [28–30] but these are based on reduced models like two- or multi-point models and are thus not necessarily sufficient. Ultimately, a reliable and predictive edge model must reproduce the full cycle of the transition from an attached regime into the fully detached regime (including also the HFSHD region observed in various metallic devices.).

With the numerical analysis of discharges in metallic tokamak devices and by removing the complexity of carbon source and transport from both, the experimental and the numerical system, some deficiencies in the understanding of the divertor physics and divertor operational conditions could be overcome and some of the most critical features which allow a robust and reliable predictions for dissipation in ITER or DEMO have been identified. For a reliable 2D power exhaust edge model the following features should be included in order to have a chance to reproduce a full cycle of the transition into detachment (with or without seeding) given only operational constraints as input parameter (system size and geometry, neutral pressure, particle throughput):

- a complete as possible kinetic neutral physics model including volume recombination, charge-exchange, and at in dense divertor conditions neutral viscosity, elastic collisions as well as molecular assisted processes and Lyman opacity
- a representative geometric model for the vessel in 2D (and if necessary in 3D), including main-chamber, divertor and sub-divertor structure that can incorporate also neutral conductance through leakages and gaps behind the PFCs up to the pumping surfaces and available pressure gauges
- cross-field drifts (i.e. ExB and grad-B drifts)
- a SOL transport model which does reflect also the advective nature of transverse transport
- an extension of simulation grid into the pedestal region in 2D to reflect the impact of X-point radiation by impurities also in the pedestal/core region and thus on pedestal pressure and P_{SOL}

For the first two features on neutral physics it is now common agreement that most of the physics processes have been included and the neutral model is complete (if not, new physics processes can be straightforwardly added due to the Monte-Carlo method being applied) there remains the more numerical question how a couple fluid-kinetic model like SOLPS-ITER can be run into convergence and what defined a good convergence metric (see discussion in [116]).

For the cross-field drifts the situation is more delicate as their inclusion into the edge model often leads to numerical difficulties and it remains to the 'pilot' of the code how to switch on drifts technically. Up to now, no clear scheme exists how to switch on drifts for example in SOLPS kind of codes and many modellers still struggle with inclusion of drift effects.

Please cite this article as: S. Wiesen et al., Plasma edge and plasma-wall interaction modelling: Lessons learned from metallic devices, Nuclear Materials and Energy (2017), http://dx.doi.org/10.1016/j.nme.2017.03.033

Anomalous transport in 2D edge codes is usually represented by fixed parameters for radial diffusion coefficients and radial advective velocities. This separation of the flux into D's and V's is not representative from the turbulence point of view [117]. Efficient and self-consistent coupling schemes of turbulence codes are still under investigation [42]. The general difficulty to validate particle flows (either turbulence- or laminar-drift-driven) is the unavailability of experimental measurements. Similarly, pedestal transport models and core boundary conditions have to be set up in a more adhoc way and normally fixed values for power and particle input into the SOL are applied either at the separatrix or close to the pedestal top without taking into account their poloidal variation.

The progress in integrated modelling using code suites like JINTRAC which couple self-consistently the various physics subsystems with different transport time-scales (i.e. core / pedestal / edge / SOL / PWI) is slow as each individual physics sub-model on its own requires careful validation. Whereas with such integrated tools transient phenomena like ELMs and fuelling dynamics can be treated at least to some extent still there is lack of suitable pedestal transport models. From integration of PWI physics there is progress underway to at least account for storage of fuel in metallic PFCs and their link to the dynamic recycling process with in the SOL.

Without having the complexity to model carbon chemical and physical sputtering, neglecting the variation in stickiness for C atoms, hydrocarbons and molecular radicals, no long range migration and carbon co-deposited layers and their erosion, metal devices seem to be simpler in terms of PWI physics compared to carbon devices. In view of integration of models taking into account PWI as well as migration of intrinsic impurities like Be or W, the edge models have been extended in order to allow for a plasma description up to the first-wall (e.g. SOLEDGE2D-EIRENE with a wide-grid option). With such upgraded integrated tools plasma flows can be better estimated which in turn can be exploited by erosion codes like ERO or global migration codes like WallDYN. Such codes have been quite successful in reproducing for example ELM-induced W-sources, impurity flows into remote areas as well as global transport and flows of extrinsic and intrinsic impurities like Be and deposition patterns. An important ingredient is a database reflecting the details on the erosion mechanisms (that is contrary to C mainly physical sputtering). Such databases are currently revised by using sophisticated molecular-dynamics codes.

Acknowledgements

This work has been carried out within the framework of the EUROfusion Consortium and has received funding from the Euratom research and training programme 2014-2018 under grant agreement No 633053. The views and opinions expressed herein do not necessarily reflect those of the European Commission.

References

[1] R. Neu, et al., Tungsten experiences in ASDEX Upgrade and JET, in: Fusion Engineering (SOFE), IEEE 25th Symposium, 2013, pp. 1–8.
[2] S. Brezinsek, et al., Nucl. Fusion 53 (2013) 083023.
[3] T. Loarer, et al., J. Nucl. Mater. 463 (2015) 1117–1121.
[4] R. Dux et al., PPCF 2014
[5] M. Wischmeier, et al., J. Nucl. Mater 463 (2015) 22.
[6] R. Schneider, Contrib. Plasma Phys. 46 (1-2) (2006) 191 3.
[7] S. Brezinsek, et al., Nucl. Fusion 55 (2015) 063021.
[8] S. Brezinsek, et al., J. Nucl. Mater 463 (2015) 11.
[9] W. Eckstein, et al., Computer Simulation of Ion Solid Interaction, Springer, Berlin, 1991.
[10] R. Behrisch, W. Eckstein, Topics Appl. Phys. 110 (2007) 33.
[11] P.C. Stangeby, J.D. Elder, Nucl. Fusion 35 (1995) 1391.
[12] A. Kirschner, Contrib. Plasma Phys. 56 (6-8) (2016) 622.
[13] J. Romazanov, et al., First application of the massively-parallel Monte Carlo code ERO2.0 for plasma-wall interaction and 3D local impurity transport at JET ILW, in: Proceedings of the 43rd EPS, Leuven, Belgium, 2016.
[14] X. Bonnin, J. Nucl. Mater. 415 (2011) S488.
[15] G. De Temmerman, Nucl. Fusion 53 (2013) 023008.
[16] M. Lehnen, et al., J. Nucl. Mater. 463 (2015) 39.
[17] J. Xiao, et al., Fusion Eng. Des. 85 (2010) 205.
[18] A. Jaervinen, et al., Plasma Phys. Control. Fusion 58 (2016) 045011.
[19] E. Wolfrum, et al., 22nd Plasma Surface Interaction Conference (PSI) this conference, 2016.
[20] C. Maggi, et al., in: 26th IAEA Fusion Energy Conference Kyoto, October, Japan, 2016, pp. 17–22.
[21] M. Dunne, et al., in: 26th IAEA Fusion Energy Conference Kyoto, October, Japan, 2016, pp. 17–22.
[22] S. Brezinsek, Phys. Scr. (2016) 014076.
[23] S. Wiesen, "Impact of the JET ITER-like wall on H-mode plasma fueling", submitted to Nuclear Fusion.
[24] M.E. Fenstermacher, et al., Plasma Phys. Contr. Fusion 41 (1999) A345–A355.
[25] V. Kotov, et al., Plasma Phys. Control. Fusion 50 (2008) 105012.
[26] S. Wiesen, et al., J. Nucl. Mater. 415 (2011) S535–S539.
[27] C. Guillemaut, et al., Nucl. Fusion 54 (2014) 093012.
[28] A. Kallenbach, et al., Plasma Phys. Control. Fusion 55 (2013) 124041.
[29] R. Goldston, et al., Plasma Phys. Control. Fusion (2017) at press: https://doi.org/10.1088/1361-6587/aa5e6e.
[30] M.L. Reinke, Nucl. Fusion 57 (2017) 034004.
[31] S. Wiesen, et al., J. Nucl. Mater. 463 (2015) 480–484.
[32] R. Simonini, et al., Contrib. Plasma Phys. 34 (1994) 368.
[33] D. Reiter, et al., J. Nucl. Mater. 196-198 (1992) 80.
[34] S. Wiesen, et al., ITC Project Report, 2006 http://www.eirene.de/e2deir_report_30jun06.pdf.
[35] H. Bufferand, et al., Nucl. Fusion 55 (2015) 053025.
[36] H. Kawashima, et al., Plasma Fusion Res 1 (2006) 031.
[37] K. Shimizu, et al., Nucl. Fusion 49 (2009) 065028.
[38] T. Rognlien, et al., J. Nucl. Mater. 196/198 (1992) 347.
[39] P.C. Stangeby, The Plasma Boundary of Magnetic Fusion Devices, Institute of Physics Publishing, Bristol, 2002.
[40] D.P. Stotler, C.F.F. Karney, Contrib. Plasma Phys. 34 (1994) 392.
[41] H. Kawashima, K. Shimizu, T. Takizuka, et al., J. Nucl. Matter. 363-365 (2007) 786–790.
[42] F.M.M. Hasenbeck, Development and Application of a Multiscale Model for the Magnetic Fusion Edge Plasma Region PhD thesis, 2016.
[43] P.C. Stangeby, Nucl. Fusion 52 (2012) 083012.
[44] D. Tskhakaya, et al., Contrib. Plasma Phys. 47 (8-9) (2007) 563.
[45] R.A. Pitts, et al., J. Nucl. Mater. 313-316 (2003) 777.
[46] M. Wischmeier, et al., J. Nucl. Mater. 313-316 (2003) 980.
[47] Y. Feng, F. Sardei, et al., J. Nucl. Mater. 313–316 (2003) 857.
[48] Y. Feng, et al., Contrib. Plasma Phys. 54 (2014) 426.
[49] O. Schmitz, et al., Nucl. Fusion 56 (2016) 066008.
[50] T. Eich, et al., Nucl. Fusion 53 (2013) 093031.
[51] B. Sieglin, et al., Plasma Phys. Control. Fusion 55 (2013) 124039.
[52] R.J. Goldston, Nucl. Fusion 52 (2012) 013009.
[53] E.T. Meier, 22nd Plasma Surface Interaction Conference (PSI) this conference, 2016.
[54] T. Eich, et al., Phys. Rev. Lett. 107 (2011) 215001.
[55] A. Loarte, et al., J. Nucl. Mater. 266-269 (1999) 587.
[56] M. Makowski, et al., Phys. Plasmas 19 (2012) 056122.
[57] B. Sieglin, et al., Plasma Phys. Control. Fusion 58 (2016) 055015.
[58] A. Scarabosio, et al., J. Nucl. Mater. 463 (2015) 49.
[59] A. Kallenbach, et al., Nucl. Fusion 55 (2015) 053026.
[60] M. Wischmeier, IAEA-FEC, St. Petersburg, Russia, 2014.
[61] G.F. Matthews, et al., Energy balance in JET, Nuclear Materials and Energy, 2016, doi:10.1016/j.nme.2016.12.012.
[62] C. Giroud, IAEA-FEC, St. Petersburg, Russia, 2014.
[63] A. Jarvinen, et al., J. Nucl. Mater. 463 (2015) 135.
[64] M. Reinke, et al., 22nd Plasma Surface Interaction Conference (PSI) this conference, 2016.
[65] S. Potzel, et al., Nucl. Fusion 54 (2014) 013001.
[66] F. Reimold, et al., Nucl. Fusion 55 (2015) 033004.
[67] F. Reimold, et al., 22nd Plasma Surface Interaction Conference (PSI) this conference, 2016.
[68] F. Reimold, et al., J. Nucl. Mater. 463 (2015) 128.
[69] L. Aho-Mantila, et al., J. Nucl. Mater. 463 (2015) 546.
[70] A. Kallenbach et al., IAEA-FEC 2012
[71] S. Varoutis, et al., in: 26th IAEA Fusion Energy Conference Kyoto, October, Japan, 2016, pp. 17–22.
[72] M. Groth, et al., J. Nucl. Mater. 463 (2015) 471.
[73] D. Moulton, et al., in: Proceedings of the 42nd EPS Conference on Plasma Physics, 2015.
[74] S. Varoutis, et al., Simulation of Neutral Gas Flow in the JET Sub-divertor and Comparison with Experimental Results, submitted to Nuclear Fusion (2015).
[75] C. Gleason-Gonzales, et al., Fusion Eng. Des. 89 (2014) 1042–1047.
[76] S. Lisgo, et al., J. Nucl. Mater. 337–339 (2005) 139.
[77] A. Kukushkin, et al., Fusion Eng. Des. 86 (2011) 2865.
[78] K. Lawson, 22nd Plasma Surface Interaction Conference (PSI) this conference, 2016.
[79] S. Wiesen, Nichtlineare Simulation von Photonentransport in Plasmen PhD thesis, 2005.
[80] V. Kotov, et al., J. Nucl. Mater. 438 (2013) S449.
[81] I. Cadez, et al., J. Phys. 133 (2008) 012029.

Please cite this article as: S. Wiesen et al., Plasma edge and plasma-wall interaction modelling: Lessons learned from metallic devices, Nuclear Materials and Energy (2017), http://dx.doi.org/10.1016/j.nme.2017.03.033

[82] W. Dekeyser, et al., 22nd Plasma Surface Interaction Conference (PSI) this conference, 2016.
[83] D. Carralero, et al., J. Nucl. Mater. 463 (2015) 123.
[84] A. Wynn, 22nd Plasma Surface Interaction Conference (PSI) this conference, 2016.
[85] B. Lipschultz, et al., Plasma Phys. Control. Fusion 47 (2005) 1559.
[86] O.E. Garcia, et al., Plasma Phys. Control. Fusion 49 (2007) B47.
[87] O.E. Garcia, 22nd Plasma Surface Interaction Conference (PSI) this conference, 2016.
[88] W. Fundamenski, et al., Nucl. Fusion 47 (2007) 417.
[89] D. Reiser, et al., Physics of Plasmas 14 (8) (2007) 082314.
[90] C. Guillemaut, et al., Nucl. Fusion 54 (2014) 093012.
[91] K. Krieger, et al., Priv. Comm., Tervaniemi Workshop, 2013.
[92] C. Bjorkas, et al., J. Nucl. Mater. 439 (1–3) (2013) 174.
[93] S. Brezinsek, et al., Nucl. Fusion 54 (2014) 103001.
[94] E. Safi, et al., J. Nucl. Mater. 463 (2015) 805.
[95] A. Kirschner, et al., J. Nucl. Mater. 463 (2015) 116.
[96] G. Sergienko, 22nd Plasma Surface Interaction Conference (PSI) this conference, 2016.
[97] K. Schmid, et al., J. Nucl. Mater. 415 (2011) 284.
[98] K. Schmid, et al., J. Nucl. Mater. 438 (2013) S484.
[99] M Mayer, et al., Phys. Scr. (2016) 014051.
[100] G. Meisl, 22nd Plasma Surface Interaction Conference (PSI) this conference, 2016.
[101] E. de la Luna, et al., IAEA-FEC, St. Petersburg, Russia, 2014.
[102] P. Tamain, et al., J. Nuc. Mat. 463 (2015) 450.
[103] D. Harting, et al., J. Nuc. Mat. 463 (2015) 493.
[104] S. Pamela, in: 26th IAEA Fusion Energy Conference Kyoto, October, Japan, 2016, pp. 17–22.
[105] R. Dux, et al., 22nd Plasma Surface Interaction Conference (PSI) this conference, 2016.
[106] M. Romanelli, et al., Plasma Fusion Res. 9 (2014) 3403023.
[107] G. Falchetto, et al., The European integrated tokamak modelling (ITM) effort: achievements and first physics results, IAEA-FEC, 2014.
[108] R. Zagorski, et al., Contrib. Plasma Phys. 48 (2008) 179.
[109] H. Shirai, et al., Plasma Phys. Control. Fusion 42 (2000) 1193.
[110] S. Wiesen, et al., 26th IAEA Fusion Energy Conference Kyoto, October, Nucl. Fus. (2016) 17–22 submitted to.
[111] M. Wischmeier, et al., J. Nucl. Mater. 363-365 (2007) 448.
[112] S. Wiesen, et al., Contrib. Plasma Phys 56 (6-8) (2016) 754–759.
[113] B. Scott, et al., Gyrokinetic theory and dynamics of the tokamak edge, in: Proceedings of the 15th Plasma Edge Theory Conference (PET), Nara, Japan, 2015.
[114] K. Schmid, Phys. Scr. (2016) 014025.
[115] D. Matveev, et al., 22nd Plasma Surface Interaction Conference (PSI) this conference, 2016.
[116] M. Baelmans, et al., 22nd Plasma Surface Interaction Conference (PSI) this conference, 2016.
[117] V. Naulin, et al., J. Nucl. Mater. 363–365 (2007) 24.

Please cite this article as: S. Wiesen et al., Plasma edge and plasma-wall interaction modelling: Lessons learned from metallic devices, Nuclear Materials and Energy (2017), http://dx.doi.org/10.1016/j.nme.2017.03.033